Technical University of Denmark

Development of Large Scale Bed Forms in the Sea –2DH Numerical Modeling

Margalit, Jonatan; Fuhrman, David R.

Publication date:
2017

Document Version
Peer reviewed version

Link back to DTU Orbit

Citation (APA):
Margalit, J., & Fuhrman, D. R. (2017). Development of Large Scale Bed Forms in the Sea –2DH Numerical Modeling. Paper presented at Coastal Dynamics 2017, Helsingør, Denmark.

DTU Library
Technical Information Center of Denmark

DEVELOPMENT OF LARGE SCALE BED FORMS IN THE SEA – 2DH NUMERICAL MODELING

Jonatan Margalit[1] and David R. Fuhrman[2]

Abstract

Large repetitive patterns on the sea bed are commonly observed in sandy areas. The formation of the bed forms have been studied extensively in literature using linear stability analyses, commonly conducted analytically and with simplifications in the governing equations. This work presents a shallow water equation model that is used to numerically simulate the morphodynamics of the water-bed system. The model includes separate formulations for bed load and suspended load, featuring bed load correction due to a sloping bed and modelled helical flow effects. Horizontal gradients are computed with spectral accuracy, which proves highly efficient for the analysis. Numerical linear stability analysis is used to identify the likely emergence of dominant finite sized bed forms, as a function of governing parameters. These are then used for interpretation of the results of a long time morphological simulation.

Key words: Bed forms, sediment transport, morphodynamics, linear stability analysis.

1. Introduction

In shallow seas, large scale bed forms consisting of non-cohesive material are commonly observed. They are typically categorized as sand waves with length O(100 m) and height O(5 m), and sand banks with length O(5 km) and height O(30 m). Some of these bed forms have repetitive patterns and seem to be actively interacting with the sea flow over the time scale of years. Field studies indicate that large scale bed forms are primarily morphologically active due to tidal currents and during storms. Sand waves have shown a tendency to migrate at a rate of several meters per year, while sand banks appear more stable with much smaller migration. These kinds of bed forms can be observed in a large part of the North Sea, and have therefore given rise to extensive studies. Human activity in the offshore environment has increased steadily over the years, and it is therefore important to understand the morphology of the sea bed from an engineering point of view. The question of how the bed forms emerged in the first place has been the subject of various theories. Research indicates that, although some bed forms may be relics from another geological period, there are also bed forms that can be explained as the result of a pure instability phenomenon of the water-bed system.

The study of large scale bed forms in shallow seas has given rise to many linear stability analyses that attempt to explain and predict field observations. These analyses are commonly conducted analytically and therefore require simplifications in the governing equations (Huthnance 1982; de Vriend 1986; de Vriend 1990; Hulscher et al. 1993; Hulscher 1996). The present work presents a complete two-dimensional horizontal (2DH) model that is used to conduct a numerical linear stability analysis, intended to identify the likely emergence of dominant finite sized bed forms, as a function of governing parameters. The work will establish fast performing 2DH numerical linear stability analyses of bed forms growth rates, utilizing a complete numerical model description. The study is both for bed load alone as well as in combination with suspended load, and includes modelled secondary current effects. The results are expected to give both quantitative and qualitative predictions, which will then be compared with subsequent morphological simulations involving the growth and migration of large-scale bed forms in the sea.

[1]Department of Mechanical Engineering, DTU, Kgs Lyngby, Denmark. jonmar@mek.dtu.dk
[2]Department of Mechanical Engineering, DTU, Kgs Lyngby, Denmark. drf@mek.dtu.dk
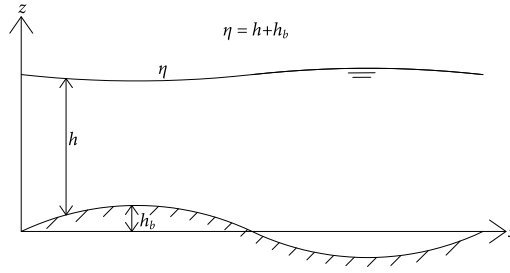
Figure 1. Definition sketch.

2. Governing Equations

2.1. *Hydrodynamics*

The hydrodynamics are described by the nonlinear shallow water equations. The wave lengths of the bed forms are several orders of magnitude larger than the depth, hence assuming shallow water conditions with only the gravitational acceleration in the vertical direction is reasonable. The governing equations for the hydrodynamics in conservative form are thus given by the depth averaged continuity equation

$$\frac{\partial \eta}{\partial t} + \frac{\partial h\overline{u}}{\partial x} + \frac{\partial h\overline{v}}{\partial y} = 0 \tag{1}$$

and the depth-averaged momentum equations

$$\frac{\partial h\overline{u}}{\partial t} + \frac{\partial h\overline{u}^2}{\partial x} + \frac{\partial h\overline{u}\,\overline{v}}{\partial y} = -gh\frac{\partial \eta}{\partial x} + f_c h\overline{v} - \frac{\tau_{bx}}{\rho} + S_x h \tag{2}$$

$$\frac{\partial h\overline{v}}{\partial t} + \frac{\partial h\overline{u}\,\overline{v}}{\partial x} + \frac{\partial h\overline{v}^2}{\partial y} = -gh\frac{\partial \eta}{\partial y} - f_c h\overline{u} - \frac{\tau_{by}}{\rho} + S_y h \tag{3}$$

where $\mathbf{u} = [\overline{u}\,\overline{v}]^T$ is the depth averaged horizontal fluid velocity vector, h is the water depth, g is the gravitational acceleration, η is the height of the water above $z = 0$, f_c is the Coriolis frequency, $\boldsymbol{\tau}_b = [\tau_{bx}\,\tau_{by}]^T$ is the bed shear stress vector, ρ is the water density and $\mathbf{S} = [S_x\,S_y]^T$ is a body force vector, which will be specified later. Horizontal stress terms have been ignored. See Figure 1 for a definition sketch. The bed shear stress is modelled using a drag coefficient C_D such that

$$\frac{\boldsymbol{\tau}_b}{\rho} = C_D \mathbf{u}|\mathbf{u}| \tag{4}$$

2.1.1. *Helical flow*

The helical flow model in this paper is based on the work of Olesen (1987), where a transport equation of the bed shear stress angle $\tan\delta_s$ is established. By introducing a right-handed streamline coordinate system, the transport equation reads

$$\frac{\partial \tan\delta_s}{\partial t} + \lambda_s \frac{\partial \tan\delta_s}{\partial s} + \tan\delta_s = -\beta \frac{h}{R_s} \tag{5}$$

where R_s is the local radius of the streamline curvature. The parameter β can be related to the flow resistance and for logarithmic flow profiles is calculated by

$$\beta = \frac{2}{\kappa^2}\left(1 - \frac{\sqrt{C_D}}{\kappa}\right) \tag{6}$$

where $\kappa = 0.4$ is the Von Karman constant. Inertial effects play a role on the intensity of the helical flow and are therefore accounted for by introducing the adaption length λ_s, defined as

$$\lambda_s = \alpha_s \frac{h}{\sqrt{C_D}} \tag{7}$$

where α_s is a calibration constant. de Vriend (1981) suggests a value of $\alpha_s = 1.3$ for helical flow intensity, however, the bed shear stress has a faster adaption and it is therefore recommended to use a value of $\alpha_s = 0.6$, in that case.

2.2. Sediment transport

2.2.1. Bed load
The bed load transport is modelled through it's relation to the bed shear stress. The total bed shear stress which acts as the total flow resistance is comprised from two contributions, as suggested by Einstein (1950): $\tau_b = \tau' + \tau''$, where the single prime accounts for skin friction on the grains and the double prime accounts for bluff body form drag due to small scale unresolved bed forms such as dunes and ripples. The bed load is assumed to be related only to the part of the bed shear stress related to skin friction, hence it is modelled from the single prime component. Engelund & Fredsøe (1976) suggest the following relation for bed load transport

$$q_b = 5P\left(\sqrt{\theta'} - 0.7\sqrt{\theta_c}\right)\sqrt{(\varsigma-1)gd^3} \tag{8}$$

where $\varsigma = 2.65$ is the specific density of sand, d is the mean grain diameter, θ' is the Shields parameter value associated with skin friction, θ_c is the Shields parameter value of incipient bed particle motion, and P is representing the probability between zero and unity, that a certain fraction of particles in a single layer are in motion. The probability P is found by

$$P = \left(1 + \left(\frac{\pi\mu_d}{6(\theta' - \theta_c)}\right)^4\right)^{-\frac{1}{4}} \tag{9}$$

where μ_d is the dynamic coefficient of motion of the sediment, estimated at 0.51.

A sloping bed affects the bed load transport as the grains are more easily transported downhill than uphill. Additionally, a transverse slope will divert the transport direction from the mean current direction. For small bed slopes in streamline coordinates, the effect is accounted for by a modification of the bed load found by Equation (8) in the following way:

$$q_{bs} = q_b\left(1 - \alpha\frac{\partial h_b}{\partial s}\right) \tag{10}$$

where and α is a coefficient estimated from

$$\alpha = \frac{3}{2}\frac{\theta_c}{\theta' - \theta_c} \tag{11}$$

The transverse bed slope effect is similarly accounted for by the equation

$$q_{bn} = q_b \left(\tan \delta_s - \theta^a G \frac{\partial h_b}{\partial n} \right) \qquad (12)$$

which also includes the deviation of the bed shear stress direction due to helical motion. The constants G and a are calibration constants estimated here to be 1.25 and -0.5, respectively.

2.2.2. Suspended load

The suspended load model is based on the Galappatti (1983) and DHI (2013) exhaustive depth-averaged solution of the sediment concentration transport equation, which corresponds to

$$\frac{\partial h\overline{c}}{\partial t} + \frac{\partial p_{mod}\overline{c}}{\partial x} + \frac{\partial q_{mod}\overline{c}}{\partial y} = \frac{\partial}{\partial x} \left(k_{xx} \frac{\partial \overline{c}}{\partial x} + k_{xy} \frac{\partial \overline{c}}{\partial y} \right) + \frac{\partial}{\partial y} \left(k_{yy} \frac{\partial \overline{c}}{\partial y} + k_{yx} \frac{\partial \overline{c}}{\partial x} \right) - E \qquad (13)$$

where $\overline{c}$ is the depth-averaged suspended sediment concentration. For the other terms see the referenced literature. The last term on the right-hand side of Equation (13) accounts for the sediment entrainment rate at the reference level from which suspended load is considered. The entrainment rate is estimated by

$$E = \phi_0 w_s \left(\overline{c}_e - \overline{c} \right) \qquad (14)$$

where ϕ_0 is the bottom value of a unit concentration profile, w_s is the mean fall velocity and $\overline{c}_e$ is the depth averaged concentration in equilibrium conditions calculated from a Rouse profile.

2.3. Bed morphology

Lastly, the rate of bed level change with time is determined by Exner equation

$$\frac{\partial h_b}{\partial t} = -\frac{1}{1-\varepsilon_p} \left(\frac{\partial q_{bx}}{\partial x} + \frac{\partial q_{by}}{\partial y} + E \right) \qquad (15)$$

where $\varepsilon_p = 0.4$ is the bed porosity

3. Numerical Methodology

The equations presented in the previous section are solved in Matlab, such that Eqs. (1), (2), (3), (5), (13) and (15) form the system of governing equations. Time integration is based on a 2nd order Runge-Kutta scheme. Horizontal gradients are computed with spectral accuracy, which proves highly efficient. The flow is driven by a body force given by

$$S_x = U_m \sigma \cos(\sigma t) + \frac{C_{D0}}{h_0} (U_c + U_m \sigma \sin(\sigma t)) \sqrt{(U_c + U_m \sigma \sin(\sigma t))^2} \qquad (16)$$

$$S_y = f_c (U_c + U_m \sigma \sin(\sigma t)) \qquad (17)$$

where U_c is the steady current velocity, U_m is the tidal velocity amplitude and σ the tidal frequency.

3.1. Linear perturbation

The linear stability analysis is performed by studying the response of the system to a small perturbation to the bed, given by a trigonometric function

$$h_b = \frac{A}{2}\sin\left(k_x x + k_y y\right) \tag{18}$$

where A is the perturbation amplitude and k_x, k_y are the wavenumbers in x and y, respectively. Assuming that the initial time development of such a perturbation with growth rate Ω and migration frequency ω is given by

$$h_b\left(x,y,t\right) = \frac{A}{2}e^{\Omega t}\sin\left(k_x x + k_y y - \omega t\right) \tag{19}$$

the linear response of the bed to this perturbation can be found by fitting the simulation results with the derivative of Equation (19), given by

$$\left.\frac{\partial h_b}{\partial t}\right|_{t=0} = \frac{A}{2}\left(\Omega\sin\left(k_x x + k_y y\right) + \omega\cos\left(k_x x + k_y y\right)\right) \tag{20}$$

In the present analysis, where responses are linear, two perturbations with opposite k_y signs are superimposed in order cope with asymmetric flow due to the Coriolis effect. The result of the growth rates are presented based on a dimensional analysis which yields a non-dimensional growth rate given by

$$\Omega^* = \frac{1}{A}\sqrt{\frac{h_0}{g}}\frac{\partial h_b}{\partial t} \tag{21}$$

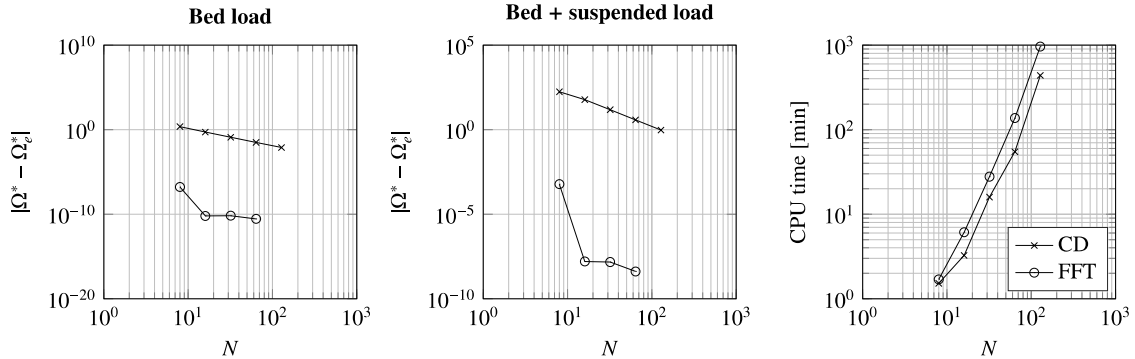where h_0 is the mean depth.

3.2. Convergence of solution

Figure 2. Comparison between a finite difference (second-order central difference) scheme (CD) and the spectral method (FFT). The left two sub-plots depict the absolute error of the non-dimensional growth rate and computational time (left: Bed load alone, center: Bed load and suspension load). Right: Computation times. The absolute error is relative to Ω_e^* which is the non-dimensional growth rate found using the spectral method with $N = 128$.

In order to investigate the rate of convergence, the spectral scheme is compared with a second-order finite difference central difference scheme. Figure 2 shows the non-dimensional growth rate and computation time vs. the number of grid points N used for discretization in each horizontal dimension, i.e. number of grid points per bed wavelength. The absolute error is relative to the error found having the spectral method with the highest number of grid points $N = 128$. The spectral method demonstrates its large advantage over the finite difference scheme as the solution is fairly accurate with as few as eight grid points resolving the bed wave. The computation time spent using the spectral method is higher than the central difference for a given domain size, however the superior accuracy of the solution with a small number of elements outweighs this expense. It can be seen that when suspended sediment transport is included, the accuracy is reduced compared to the bed load alone. This is due to the vertical integration of the concentration profiles, which is only accurate up to second order, thus limiting efficiency of the spectral method. It is however

substantially better than all the results produced by the finite difference scheme. Based on this analysis it is chosen to conduct all further simulations with the spectral method using $N = 16$ grid points to resolve the bed wave in each direction.

4. Results

Table 1 lists the parameters of the studied case, in which the current velocity, depth, resistance and grain diameter serve as model inputs, where the zero subscript represents the unperturbed values. For each forthcoming figure presenting linear stability contours for the non-dimensional bed growth Ω^*, 400 simulations have been conducted on a HPC cluster for a variety of dimensionless wavenumbers $k_x h_0, k_y h_0$ spanning the range 0 to 0.3. In the following a comparison between a steady current and a unidirectional tidal flow is presented, followed by a look at the effects of the bed load bottom slope correction and the helical flow model. Lastly, based on the results on the linear stability analysis, the morphological development of a bed is presented.

Table 1. Simulation parameters.

Current velocity U_0	Depth h_0	Drag coefficient C_{D0}	Grain diameter d	Skin friction Shields parameter θ_0	Rouse number Z_0	Suspended / Bed load ratio q_{s0}/q_{b0}
1 m/s	30 m	0.00459	0.250 mm	0.24	1.05	1

4.1. *Steady current vs. tidal current*

Linear stability analysis of tidal bed forms is commonly studied by separation of the hydrodynamic and the morphological time scales, such that updates of the bed are performed by averaging the sediment transport over a full tidal cycle (Huthnance 1982; de Vriend 1990; Hulscher 1996). The Coriolis effect creates an asymmetric flow, which usually yields anti-clockwise directed bed forms in the northern hemisphere. Zimmerman (1981) links this phenomenon to clockwise circulating residual flow cells around the crests, where the upstream velocity is slightly larger than the downstream. As mentioned previously, the doubly-periodic bed form allows the simulation of both negative and positive k_y wave numbers in a single simulation. Figure 3 shows a comparison between two flow conditions. One, where a steady current is used ($U_c = 1$ m/s and $U_m = 0$ m/s), and a second, where an M2 tide with frequency $\sigma = 1.4053 \cdot 10^{-4}$ rad/s is simulated ($U_c = 0$ m/s and $U_m = 1$ m/s) and the growth rate is found by averaging over the tidal period. The upper plots show the non-dimensionalized growth rate contours with bed load only, while the lower show it for combined bed load and suspended load. The peak ($k_x h_0, k_y h_0$) positions are marked with a dot for a given set, with the peak growth rates Ω^* indicated. Negative contours, i.e. decaying bed forms have been omitted from the plots.

Figure 3 shows that in all four cases the peaks are highest in regions with negative $k_y h_0$ values, i.e. fastest growing anti-clockwise directed bed forms. Over half a period, the tidal flow has a lower averaged velocity than the steady current case, which manifests itself in the magnitude of the peaks. It can be seen that in bed load only simulations there is a factor 2.5 between the two flow conditions, while it is roughly factor 3.5 when suspended load is included. The ratio of the peaks between the positive and negative $k_y h_0$ regions is around 1.3 for the bed load alone and 1.5 including the suspended load. One important attribute of the suspended load inclusion is that the growth contours now span a lower range of the wavenumber $k_x h_0$, while maintaining the $k_y h_0$ range. This suggests that suspended load suppresses the evolution of shorter wave lengths and also tends to result in bed forms which are more aligned with the mean flow direction. For the bed load alone, the contours in both flow conditions show a similar form and peaks located at $(k_x h_0, k_y h_0) = (0.091, -0.115)$ for steady current and $(k_x h_0, k_y h_0) = (0.079, -0.099)$ for the tidal flow. This corresponds to wave lengths of O(1 km) rotated approximately 38° to the mean current direction, i.e. short sand banks. In the cases where suspended load is included a difference in the contour shapes is more observable and the peaks are located at $(k_x h_0, k_y h_0) = (0.023, -0.055)$ for steady current and
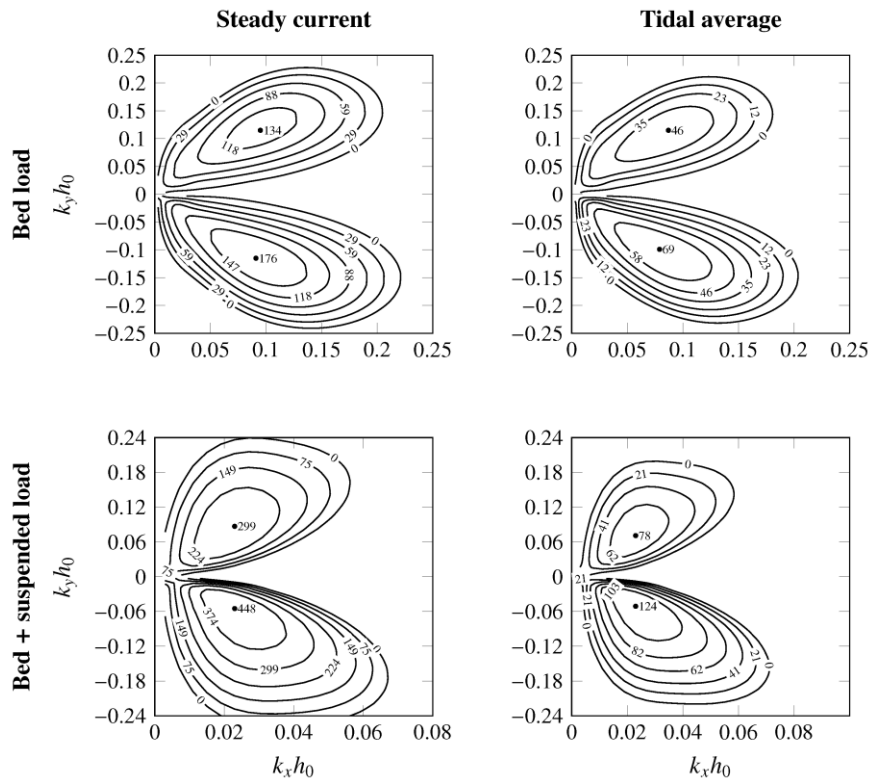
Figure 3. Steady current vs tidal current. Non-dimensional growth rate $\Omega^* \cdot 10^{11}$, with bed load alone and combined with suspended load. Note the different scaling of the axes.

$(k_x h_0, k_y h_0) = (0.023, -0.051)$ for the tidal flow. This corresponds to wave lengths of O(3 km) rotated approximately 23° to the mean current direction, i.e. also characterized as sand banks.

These results suggest that replacing a tidal flow with a steady current for the obtaining growth rates using linear stability analysis seems to be a viable approach. This has also been confirmed through similar testing of other cases. In literature, it is common to see studies that disregard the suspended load or include it in a total load model. Whichever transport model chosen, it seems that the linear growth rates only differ quantitatively while being qualitatively the same. The main advantage of the steady current over the tidal current, is a much shorter computational time.

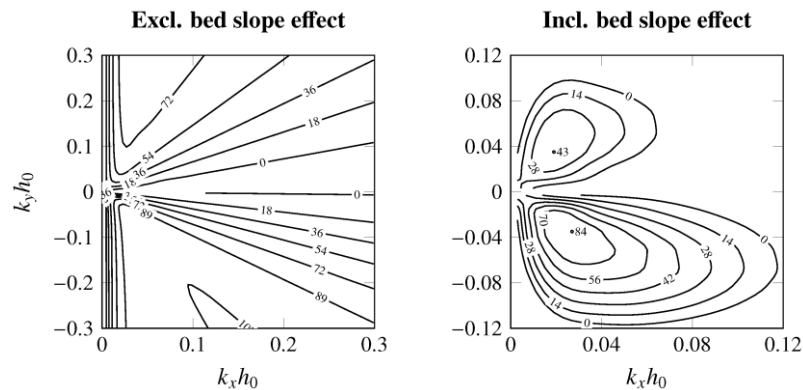### 4.2. *Bed slope effect*

Figure 4. Effect of bed slope. Non-dimensional growth rate $\Omega^* \cdot 10^{11}$ with bed load alone. Note the different scaling of the axes.

In this section, the model is used to test how the bottom slope correction of the bed load given by Equations (10) and (12) affects the stability of the bed forms. For this the model is simulated with bed load only and the helical flow model is deactivated. Figure 4 shows the non-dimensional growth rate contours from simulations including and excluding the bed slope correction of the bed load transport. It can be seen that the inclusion of the bed slope correction is essential to achieve a closed peak. This numerical solution supports the conclusion of de Vriend (1986) that the system is entirely unstable without the slope effect, while inclusion of it dampens the growth, mostly of shorter wave-lengths since they have steeper slopes.
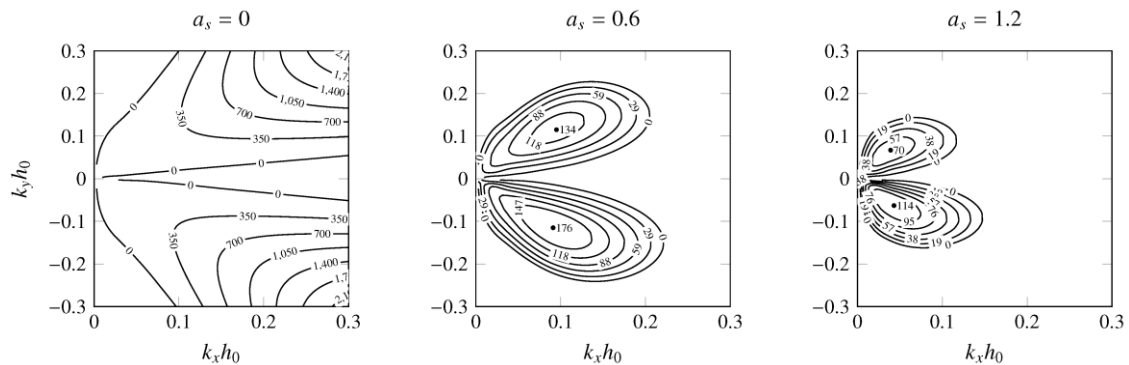
4.3. *Helical flow effect*

Figure 5. Effect of adaption length in the helical motion model on the unstable growth rate. Non-dimensional growth rate $\Omega^* \cdot 10^{11}$ with bed load alone. Note the different scaling of the axes.

In this section, the model is used to study the influence of the helical flow on the stability of the bed forms. Although the effect has influence on both the bed and suspended load transports, it is here tested with bed load only for simplicity; Qualitatively similar results have been found when suspended load is included. Figure 5 shows the effect of setting the adaption length coefficient in the Equation (7) to $\alpha_s = 0, 0.6, 1.2$. The case with zero adaption length means that essentially the flow responds immediately without any adaption to varying flow conditions. This can be seen by the left contour plot where no peak emerges within the studied range, and the growth rate increases with increasing wavenumbers. When the adaption length is included, as in the center and right plots, the higher wavenumbers become stable (i.e. decaying bed forms) and a peak growth mode emerges, while the magnitude of the growth rate is reduced. From a physical perspective, the lateral bed slope effect causes the bed load transport vector to veer downslope and the helical water motion causes it to veer up-slope. This balance between these two effects is clearly visible when sequentially considering the plots from left to right, where the helical flow effect is reduced as the contours become more asymmetric. The next plot in this sequence would be the right plot in Figure 4, which could represent the case of $\alpha_s \rightarrow \infty$, i.e. no helical flow correction of the bed load transport. The sequence shows that with no adaption length, the helical flow is dominating the bed load vector and causes enhanced bed form development by carrying sediments from troughs to crests, generating steep slopes and shorter wave lengths. The adaption length retards this effect, which is the reason why the growth rate magnitude is reduced and peaks appear at lower wavenumbers. Increasing the adaption length also yields more asymmetry around $k_x h_0$. This is due to a balance between the Coriolis effect and the helical flow effect. Hulscher et al. (1993) adopted a similar approach and used an adaption length coefficient of 0.6. Their model was able to show qualitatively how a dominant mode yielding a short-waved bed form nearly perpendicular to the mean flow direction could emerge. The current results yield wave lengths on the order of 1-3 km and bed form to current angle of 20°– 40°, which as previously mentioned, can be characterized as sand banks.

4.4. *Morphology*

The results of the linear stability analysis are now put to a test in order to see how the model performs when the bed is allowed to evolve. Using the flow conditions listed in Table 1, a simulation is performed

for a domain size corresponding to the wavenumber of the highest peak in Figure 3 for bed load and steady current, i.e. $(k_x h_0, k_y h_0) = (0.091, -0.115)$. A normally distributed random bed perturbation with standard deviation of 1% of the mean depth is introduced initially, on a 16×16 grid. The initial bed condition is depicted in the left of Figure 6. In order to speed up the morphology, the rate of bed level change $\partial h_b / \partial t$ is amplified by a factor 10,000. Figure 7 shows the maximum bed level and the root mean square of the bed over the simulation period.

Figure 6 (center) shows the bed in the early morphological stages where it can be seen that linear sinusoidal bed forms have emerged with the wavenumbers as predicted by the linear stability analysis. This corresponds to the exponential growth stage seen in Figure 7 between $100 - 200$ years. This matches very well the evolution described by Equation (19). As the bed is allowed to continue morphing it becomes nonlinear and reaches an equilibrium stage at the 300 years mark, with shape depicted on Figure 6 (right). From this stage on, the bed remains growth neutral and only migrates. It can be seen that the bed form appears to be nearly doubly periodic, which can be attributed to the second mode which had a slower evolution, thus needing more time to evolve. This mode corresponds very well to the second peak in Figure 3 (steady current – bed load) in the positive $k_y h_0$ region.
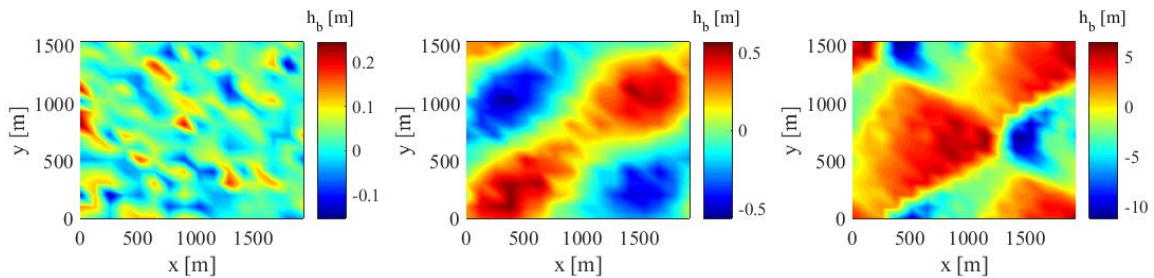

Figure 6. Bed level evolution for bed load alone simulation. Left: initial randomly perturbed bed. Center: Linear bed forms at early stage of development. Right: Fully developed stable bed form.
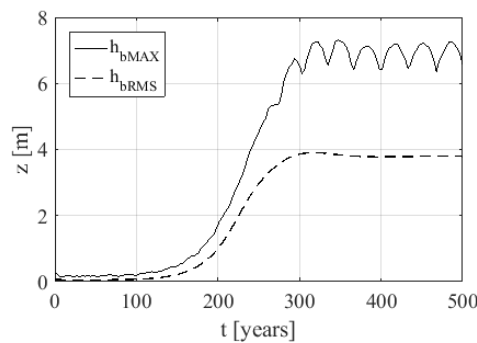

Figure 7. Time development of maximum elevation and root mean square of the bed elevation. Results are from a bed load alone simulation.

Naturally imposing the domain size and the grid density limits the spectrum of the possible outcomes of the previous simulation. This is tested further here for the model, now including the suspended load. The domain is now prescribed by the wavenumber set $(k_x h_0, k_y h_0) = (0.023, -0.055)$, corresponding to the peak in Figure 3 for the total load and steady current. As before the bed is perturbed randomly, while the rate of bed level change is amplified by a factor 2000. Figure 8 (left) shows very clearly a linear bed form emerging with the expected wavenumber values. On Figure 8 (right) the domain size is doubled in each direction. It can now be seen that the bed forms have some discontinuities, but the emerged bed forms have the same wavenumber values as predicted by the linear stability analysis, and as depicted on Figure 8 (left).

The corresponding time development of the bed height is shown in Figure 9, where it can be seen that in this case the bed does not reach an equilibrium in terms of growth, and the bed evolution occurs much faster than in the bed load alone case, in line with expectations based on the linear stability analysis.
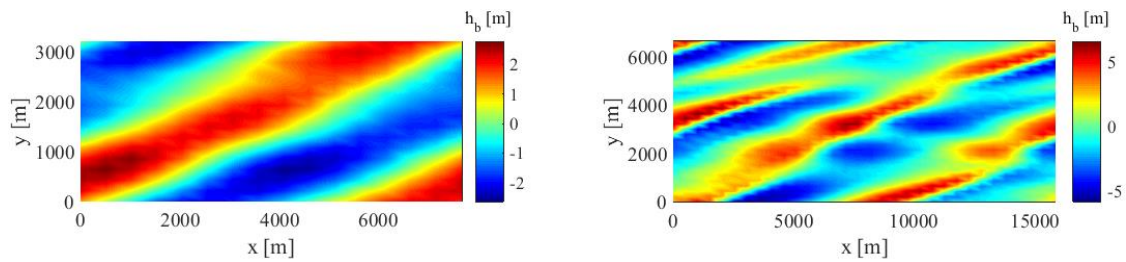
Figure 8. Bed level for bed and suspended load simulations. Left: domain with single bed form. Right: domain of twice the size showing emergence of two bed forms.
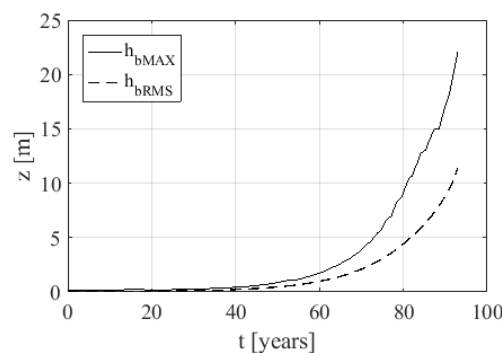

Figure 9. Time development of the maximum elevation and root mean square of the bed elevation. Results are from a combined bed and suspended load simulation.

5. Conclusions

A shallow water model with helical flow effects and sediment transport has been developed in order to simulate the sea bed morphodynamics, in a similar fashion as in modern commercial models. The model utilizes a spectral method, which proves to be extremely efficient for a desired accuracy on a periodic domain. The model has been used to study the effects of bottom slope and helical flow motion on the sediment transport, in a numerical linear stability analysis. The simulations were performed with a steady current which has been shown to give qualitatively similar results to those obtained in a unidirectional tidal flow. Results have shown that suspended load modeling yields quite different results than bed load alone on the emergence of bed forms, and is therefore important to consider. It has been demonstrated numerically that inclusion of a bottom slope correction of the bed load must be incorporated in order to achieve stable results. This is in line with analytical findings in literature. Furthermore, the helical flow, which effects the direction of the bed shear stress and hence the sediment transport direction, has a significant influence on the characteristics of the emerging bed forms. It counter-balances the Coriolis force, such that this balance of the terms can determine if the outcome is symmetric or asymmetric.

The linear stability analysis yielded dominant bed forms of wave-lengths 1–3 km rotated 20°–40° relative to the mean flow direction, which is characteristic of large sand banks. These results were used to select a domain size which was then introduced to a small random perturbation for a morphological simulation. Both for a bed load alone and with suspended load the simulations yielded the bed forms that were predicted by the linear stability analysis. The bed load alone morphology reached equilibrium, such that the bed form stopped growing and only migrated, while the bed form computed with suspended load did not reach an equilibrium condition. Altogether, the analysis and subsequent morphology simulation combine to demonstrate both the initial formation of bed forms from a completely random bed and longer term evolution. By amplifying the morphological growth, decades and centuries of evolution can be simulated with the present model in a matter of hours.

References

DHI, 2013. MIKE 21 & MIKE 3 Flow Model FM - Sand Transport Module - Scientific Documentation.

Einstein, H.A., 1950. The Bed-Load Function for Sediment Transportation in Open Channel Flows. *Soil Conservation Service*, (1026), pp.1–31.

Engelund, F. & Fredsøe, J., 1976. A Sediment Transport Model for Straight Alluvial Channels. *Nordic Hydrology*, 7(5), pp.293–306.

Galappatti, R., 1983. *A depth integrated model for suspended transport*,

Hulscher, S.J.M.H., 1996. Tidal-induced large-scale regular bed form patterns in a three-dimensional shallow water model. *Journal of Geophysical Research*, 101(C9), p.20727.

Hulscher, S.J.M.H., de Swart, H.E. & de Vriend, H.J., 1993. The generation of offshore tidal sand banks and sand waves. *Continental Shelf Research*, 13(11), pp.1183–1204.

Huthnance, J.M., 1982. On one mechanism forming linear sand banks. *Estuarine, Coastal and Shelf Science*, 14(1), pp.79–99.

Olesen, K.W., 1987. *Bed topography in shallow river bends*. Delft University of Technology.

de Vriend, H.J., 1986. 2DH computation of transient sea bed evolutions. In *20th Coastal Engineering Conference*. pp. 1698–1712.

de Vriend, H.J., 1990. Morphological processes in shallow tidal seas. *Residual Currents and Long-Term Transport, Coastal Estuarine Studies*, 38(June), pp.276–301.

de Vriend, H.J., 1981. Steady flow in shallow channel bends. *Comm. on Hydr. Engrg, Dept. of Civil Engrg, Delft University of Technology, Report*, 81–3.

Zimmerman, J.T.F., 1981. Dynamics, diffusion and geomorphological significance of tidal residual eddies. *Nature*, 290(5807), pp.549–555.